ACS APPLIED MATERIALS & INTERFACES

Research Article

www.acsami.org

3D Graphene Functionalized by Covalent Organic Framework Thin Film as Capacitive Electrode in Alkaline Media

Zeqi Zha,[†] Lirong Xu,[†] Zhikui Wang,[‡] Xiaoguang Li,[†] Qinmin Pan,[‡] Pingan Hu,[†] and Shengbin Lei*[,†]

[†]Key Laboratory of Microsystems and Microstructures Manufacturing, Ministry of Education, and [‡]State Key Laboratory of Robotics and System, Harbin Institute of Technology, Harbin 150080, P. R. China

Supporting Information

ABSTRACT: To harness the electroactivity of anthraquinone as an electrode material, a great recent effort have been invested to composite anthraquinone with carbon materials to improve the conductivity. Here we report on a noncovalent way to modify three-dimensional graphene with anthraquinone moieties through on-surface synthesis of two-dimensional covalent organic frameworks. We incorporate 2,6-diamino-anthraquinone moieties into COF through Schiff-base reaction with benzene-1,3,5-tricarbaldehyde. The synthesized COF -graphene composite exhibits large specific capacitance of 31.7 mF/cm^2. Long-term galvanostatic charge/discharge cycling experiments revealed a decrease of capacitance, which was attributed to the loss of COF materials and electrostatic repulsion accumulated during charge−discharge circles which result in the poor electrical conductivity between 2D COF layers.

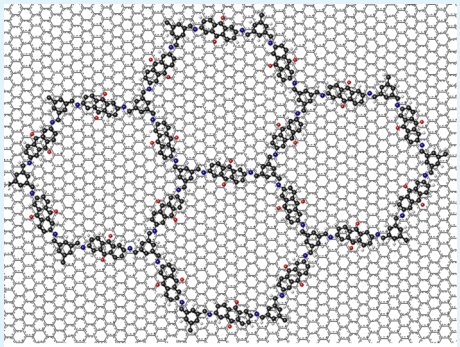

KEYWORDS: *covalent organic framework, anthraquinone, alkaline electrolyte, noncovalent functionalization, graphene, capacitor*

INTRODUCTION

Anthraquinone-based materials are one of the most important examples of organic redox couples.[1] They have attracted wide interest in the broad field of energy storage and conversion. For instance, anthraquinone derivatives have been used as oxygen reduction electrocatalyst,[2] electrochemical capacitors[3,4] and polymer−air battery.[5] However, the bad conductivity of anthraquinone limits its development as an electrode material. So, many efforts have been paid to composite anthraquinone with carbon materials, which are the traditional good conductive electrode material. The primary method for modification of carbon materials with anthraquinone is based on spontaneous reduction of the in situ generated diazonium derivative on active carbon or graphene.[6,7] The advantage of this approach is that the anthraquinone and carbon materials are connected with covalent bonds, which leads to good conductivity between them. However, the disadvantage of this approach is that the loading mass of anthraquinone is low and there are many unreacted anthraquinones physically adsorbed on the carbon material, which could lead to bad cycle stability.[7,8]

Covalent organic frameworks (COFs) are two-dimensional or three-dimensional porous crystalline networks whose molecular building blocks are linked by covalent bonds, provide robust materials that allow uniform nanometer-scale pores and predictive design criteria to organize functional building blocks.[9−11] 2D COFs with high specific surface area and layered structures stacked together through $\pi-\pi$ interactions are ideally suited for efficient energy storage and charge transport.[11] Incorporation of anthraquinone moieties into 2D COFs may achieve high theoretical energy density because the continuous, ordered pores of 2D COFs may facilitate ion transport. Recently, Dichtel's group has reported a significant work where an anthraquinone-containing 2D COF powder binded with carbon black was used as an electrode material, which exhibit higher capacitance than those modified with nonredox-active COF. However, only 2.5% of the anthraquinone moieties was accessed in this 2D COF slurry modified electrode, which was attributed to the random orientation of polycrystalline COF particles and nonoptimal interface to the bulk electrode.[12] In one of our recent works, we have demonstrated that single-layer 2D COF can be synthesized on graphene surface through on-surface condensation between aromatic aldehyde and amine.[13] DFT simulations have confirmed the strong interaction and significant electron band mixing between the well oriented single layer COF and graphene. Taking into account the good conductivity of graphene, this inspired us that incorporation of anthraquinone containing COF films with graphene via on-surface synthesis may lead to well oriented 2D COF films with good conductive contact with graphene due to van der Waals epitaxy effect, providing an opportunity to significantly improve the accessibility of anthraquinone moieties. Here, we report a new procedure that can incorporate π-conjugated surface COF with anthraquinone moiety onto 3D graphene through a noncovalent way. The electrode obtained in this way has good

Received: May 14, 2015
Accepted: July 23, 2015
Published: July 23, 2015

DOI: 10.1021/acsami.5b04185
ACS Appl. Mater. Interfaces 2015, 7, 17837−17843

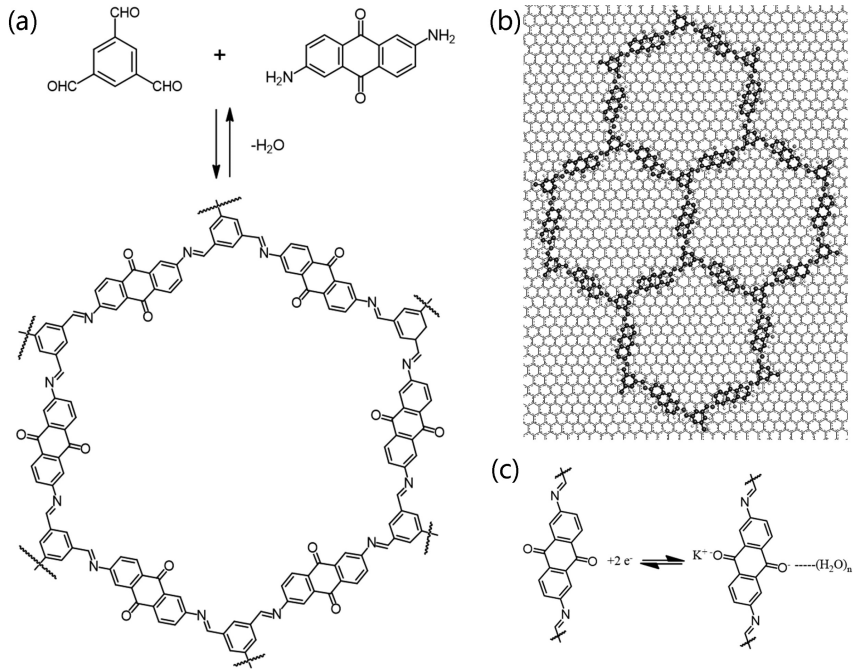

Figure 1. (a) Synthesis of $COF_{DAAQ\text{-}BTA}$, (b) geometrical structures of surface $COF_{DAAQ\text{-}BTA}$ on graphite. (c) Redox reaction of anthraquinone in alkaline media of KOH aqueous solution, the charge of the reduced form is compensated by hydrogen bonds and alkaline cations (e.g., K^+).

quality of conductivity, and multilayer COF films can be obtained which result in the larger anthraquinone loading mass. The synthesized $COF_{DAAQ\text{-}BTA}$-graphene composite exhibits large specific capacitance of 31.7 mF/cm^2 with an improved accessibility of 13.45% of the anthraquinone moieties in an alkaline media.

2. EXPERIMENTAL SECTION

Synthesis of $COF_{DAAQ\text{-}BTA}$-3DG. Utilizing nickel foam (1.5 × 1.5 × 0.15 cm^3, Shanghai Zhongwei New Material Co., Ltd.) as template and catalyst, three-dimensional graphene (3DG) was synthesized via a modified CVD method.[14] Without dissolving nickel, 3DG was directly used to prepare the composite material of $COF_{DAAQ\text{-}BTA}$-3DG. The $COF_{DAAQ\text{-}BTA}$-3DG was synthesized by an interfacial polymerization method. The typical procedure was as follows: 2,6-diaminoanthraquinone (DAAQ) and benzene-1,3,5-tricarbaldehyde (BTA) were dissolved in dimethylacetamide with a mass concentration of 2.2 and 1.0 mg/g, respectively. With a mole ratio of about 3:2, 370 μL of mixed solution was obtained. Simultaneously, 6% volume ratio of deionized water was added to the mixture. Then the resulting suspension was directly used to soak the 3DG. The composite was heated at 140 °C for 5 h and annealed at 205 °C for 1 h under an argon atmosphere. The loaded weight of the $COF_{DAAQ\text{-}BTA}$ on the 3DG was about 0.253 ± 0.015 mg/cm^2. For the control experiment, the working electrode modified with DAAQ monomer was achieved by soaking 3DG in a saturated solution of DAAQ in tetrahydrofuran for 10h at 25 °C. This resulted DAAQ loading mass on 3DG was about 0.053 ± 0.014 mg/cm^2. Longer soak time (up to 24 h) did not increase the DAAQ loading.

Characterization. For scanning tunneling microscopy (STM) characterization, the surface $COF_{DAAQ\text{-}BTA}$ was prepared on highly oriented pyrolytic graphite (HOPG) surface. In this case DAAQ and BTA were dissolved in dimethylacetamide with a mass concentration of 0.01 mg/g, with mole ratio of 4:1. Deionized water was added with 6% volume ratio to the mixed solution. Then 4 μL of the mixture was drop-casted on HOPG surface. The sample was annealed in a vacuum oven at 140 or 205 °C for 30 min with a pressure of <133 Pa. STM measurements were carried out using an Agilent 5100 scanning probe microscope with mechanically formed Pt/Ir (80/20) tips under ambient conditions. All STM images were taken in the constant current mode. AFM measurements of the $COF_{DAAQ\text{-}BTA}$-3DG composite were performed with a Bruker multimode 8 AFM equipped with a Nanoscope V controller. Antimony(n) doped Si (model RTESP, part MPP-11100−10, Bruker) cantilever with a resonant frequency of 309−343 kHz and spring constant of about 20−80 N/m were used in imaging by noncontact mode. X-ray photoelectron spectroscopy (XPS) analysis was performed with a PerkinElmer PHI 5400 ESCA system with standard Al Kα (1486.6 eV) irradiation (narrow scan, pass energy is 22.35 eV). UV−vis spectra were obtained with a TU-1800SPC UV-vis spectrometer (Purkinje General Instrument). Fourier transform infrared (FTIR) spectra of DAAQ and BTA were measured with a PerkinElmer Spectrum-100 FTIR spectrophotometer, whereas the spectrum of the $COF_{DAAQ\text{-}BTA}$-3DG composite was obtained on a Thermo-Fisher Nicolet 6700 instrument with attenuated total reflectance (ATR-FTIR) mode.

Electrochemical Measurements. The electrochemical analyses were performed in a standard three-electrode system, in which platinum foil and Ag/AgCl electrodes were used as counter and reference electrodes, respectively. The $COF_{DAAQ\text{-}BTA}$-3DG sample was directly used as the working electrode with the nickel foam as current collector. Before analyses, the electrolyte (1 mol/L KOH in deionized water) was purged with ultrahigh pure argon for 1h, and during all the electrochemical analyses, the three-electrode system was under argon atmosphere. All solutions were prepared with deionized water purified with a Milli-Q system (18.2 MΩ cm). All potentials are referred to Ag/AgCl electrode. Prior to any

DOI: 10.1021/acsami.5b04185
ACS Appl. Mater. Interfaces 2015, 7, 17837−17843

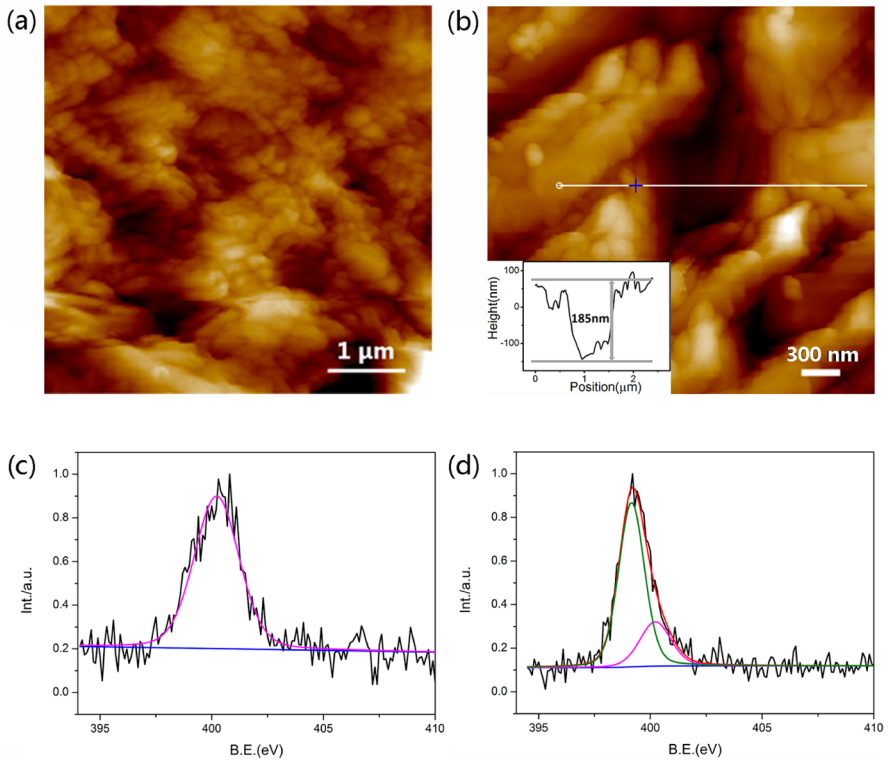

Figure 2. (a) AFM image of $COF_{DAAQ\text{-}BTA}$-3DG composite, (b) AFM image of scratched $COF_{DAAQ\text{-}BTA}$-3DG composite and the corresponding section profile, (c) XPS spectra of N 1s of DAAQ monomer, and (d) $COF_{DAAQ\text{-}BTA}$-3DG composite.

measurement, the working electrode was dipped in the electrolyte for 40 min for the purpose of allowing the electrolyte to impregnate the electrode porosity. The cyclic voltammetry measurements, chronoamperometry and galvanostatic charge−discharge test were performed on a CHI 660D electrochemical workstation (Chenhua, Shanghai, China) at 25 °C. The capacitances were calculated from galvanostatic charge−discharge experiments using the discharge potential−time curve using eq 1:

$$C = I\Delta t/(\Delta VA) \quad (1)$$

where C (mA/cm^2) is specific capacitance, ΔV (V) represents potential drop during discharge, A (cm^2) designates the apparent area of the working electrode, Δt (s) is the total discharge time, and I (mA) represents discharge current.

3. RESULTS AND DISCUSSION

Synthesis and Characterization of Surface $COF_{DAAQ\text{-}BTA}$. The $COF_{DAAQ\text{-}BTA}$ was achieved by condensation between DAAQ and BTA (illustrated in Figure 1a). As depicted in Figure 1a, aldehyde group and amine group undergo condensation reaction to form a Schiff-base bond by removing one water molecule.[15] The geometrical structures of surface $COF_{DAAQ\text{-}BTA}$ is presented in Figure 1b.

It has been reported that adding water to the reaction solution is necessary to obtain high quality surface COFs.[16,17] The existence of water provides slightly reversible reaction condition, can push the dehydration reaction backward to promote self-repairing process. Thus, 6% volume ratio of deionized water was added to the mixture when preparing the surface $COF_{DAAQ\text{-}BTA}$-3DG composite. To characterize the morphology of the surface $COF_{DAAQ\text{-}BTA}$-3DG composite, atomic force microscopy (AFM) was performed on flat terraces of the composite. The AFM morphology of surface $COF_{DAAQ\text{-}BTA}$ reveals much higher surface roughness in comparison with bare graphene, as shown in Figure 2a. There are a lot of features with lateral size of 50 to 100 nm (Figure 2a), while in case of 3DG, most of the surfaces are flat and featureless except wrinkles are visible in some area (Figure S1). To evaluate the thickness, the surface $COF_{DAAQ\text{-}BTA}$ was scratched by contact mode scans at a zoomed-in area of 500 nm × 500 nm in size.[18] Amplitude set point of 2 V was applied during the contact mode scans. Then the surface morphology was collected over the original 3 μm × 3 μm area with tapping mode again. A nearly square-shaped recessed area of 500 nm × 500 nm in size is observed (Figure 2b). Further scraping did not change the surface of inner square area anymore, which means no more COF can be moved after reaching the surface of 3DG. From the section profile, the scratch experiment indicates that the thickness of the COF film is about 180 nm.

X-ray photoelectron spectroscopy (XPS) was used to confirm the formation of the multilayer $COF_{DAAQ\text{-}BTA}$ film (Figure 2). XPS spectra for the DAAQ monomer are characterized by the presence of N 1s at 400.22 eV, whereas N 1s peak of $COF_{DAAQ\text{-}BTA}$-3DG composite can split into two peaks located at 399.34 and 400.22 eV, respectively. The peak at 399.34 eV is assigned to the N in the imine bond, whereas the peak at 400.22 eV to NH_2 in the monomer. These assignments of relative peak positions are in agreement with previous studies.[19] The peak area at 400.22 eV is about one-third of that of the one at 399.34 eV, which indicates that about 25% of the DAAQ exist as unreacted monomer. The FTIR spectrum of the $COF_{DAAQ\text{-}BTA}$-3DG composite (Figure S2) also confirms the existence of unreacted monomers.

Though the AFM and XPS characterizations proves the formation of $COF_{DAAQ\text{-}BTA}$ on the graphene surface, these

DOI: 10.1021/acsami.5b04185
ACS Appl. Mater. Interfaces 2015, 7, 17837−17843

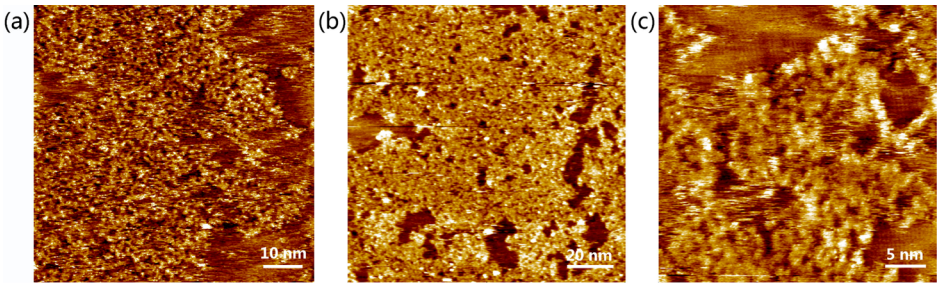

Figure 3. (a) STM image of surface $COF_{DAAQ\text{-}BTA}$ on HOPG prepared at 140 °C. (b) Large-scale and (c) high-resolution STM image of surface $COF_{DAAQ\text{-}BTA}$ on HOPG prepared at 205 °C.

techniques cannot provide real space structural information on the $COF_{DAAQ\text{-}BTA}$ with atomic precision. For this purpose scanning tunneling microscopy (STM) is the technique of choice, which has been repeatedly corroborated its ability in providing structural details with atomic precision in supramolecular and covalent nanostructures.[15,20−23] As we know, HOPG and graphene have the similar lattice structure.[24] Thus, we use HOPG instead of 3DG to characterize the morphology of $COF_{DAAQ\text{-}BTA}$. For the sample prepared by heating at 140 °C for 30 min, extended adlayer of π-conjugated surface $COF_{DAAQ\text{-}BTA}$ were revealed by STM (Figure 3a). However, the surface coverage is insufficient and the continuity of the surface $COF_{DAAQ\text{-}BTA}$ is also not good, which indicates the reaction is incomplete. The following electrochemical test also confirms the incomplete covalent linking of the network, where $COF_{DAAQ\text{-}BTA}$ of the working electrode easily fells off into the electrolyte during the electrochemical characterization. To improve the stability of surface $COF_{DAAQ\text{-}BTA}$, the reaction temperature was raised to 205 °C. As shown in Figure 3b, c, STM images show a high coverage with better continuity. Figure 3c is a high-resolution STM image that shows the pores of $COF_{DAAQ\text{-}BTA}$. The structure of the pores is not very clear, and we attributed to the filling of pores by excess of DAAQ monomers which can bind with the network through hydrogen bond and dipole−dipole interactions. From the STM characterization we can say that the on-surface condensation has successfully resulted in a continuous 2D polymer containing anthraquinone moieties; however, the network is not periodic and the structure is amorphous rather than crystalline.

Electrochemical Measurements. The electrochemical behavior of anthraquinone in electrolyte with different pH has been well studied in previous reports.[1,8] The redox reaction of anthraquinone in alkaline electrolyte is illustrated in Figure 1c. In the reduced form, two electrons transfer to each anthraquinone and the charges are compensated by water molecules or cationic species (Figure 1a) .[8]

The cyclic voltammogram of 3DG, DAAQ monomer modified 3DG and $COF_{DAAQ\text{-}BTA}$-3DG composite are shown in Figure 4, respectively. The CV of 3DG shows a typical rectangular shape, characteristic of carbon materials (Figure 4a). There is no oxygen reduction peaks appeared between −0.8 and −1.05 V, which has been observed in a previous report.[25] This means the oxygen concentration in the electrolyte is close to zero under argon atmosphere. As shown in Figure 4b, the DAAQ monomer modified working electrode (with DAAQ loading mass of 0.053 mg/cm^2) was characterized by the oxidation and reduction peaks at −0.772 V and −0.877 V, respectively. Comparing the CV of 3DG with that of DAAQ monomer modified 3DG, because the peak area is quite small, the modification with physisorbed DAAQ monomer does not significantly increase the capacitance of the 3DG electrode.

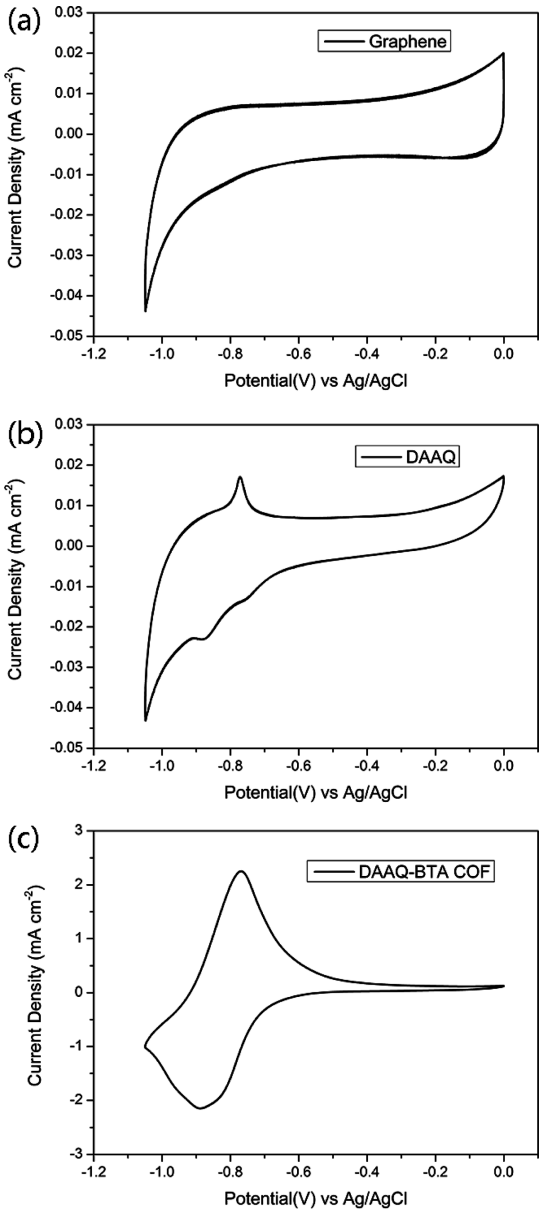

Figure 4. Cyclic voltammogram of (20 mV/s, 1 mol/L KOH) (a) bare 3DG working electrode, (b) DAAQ monomer-3DG working electrode, and (c) $COF_{DAAQ\text{-}BTA}$-3DG working electrode.

The oxidation of $COF_{DAAQ\text{-}BTA}$-3DG appears at −0.769 V with a oxidation current of ~2.2 mA/cm^2, whereas its reduction

DOI: 10.1021/acsami.5b04185
ACS Appl. Mater. Interfaces 2015, 7, 17837−17843

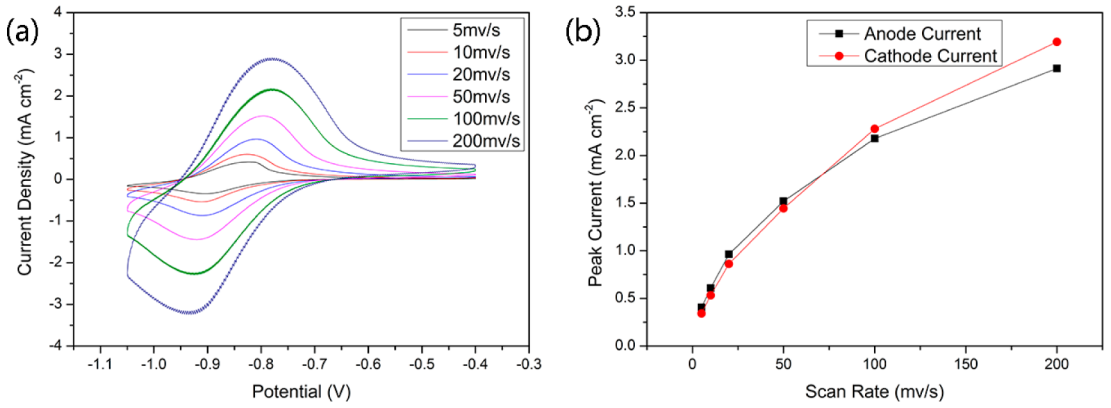

Figure 5. CV curves of $COF_{DAAQ\text{-}BTA}$-3DG at different scan rates in 1 mol/L KOH electrolyte (a) and the relationship of peak current with scan rate (b).

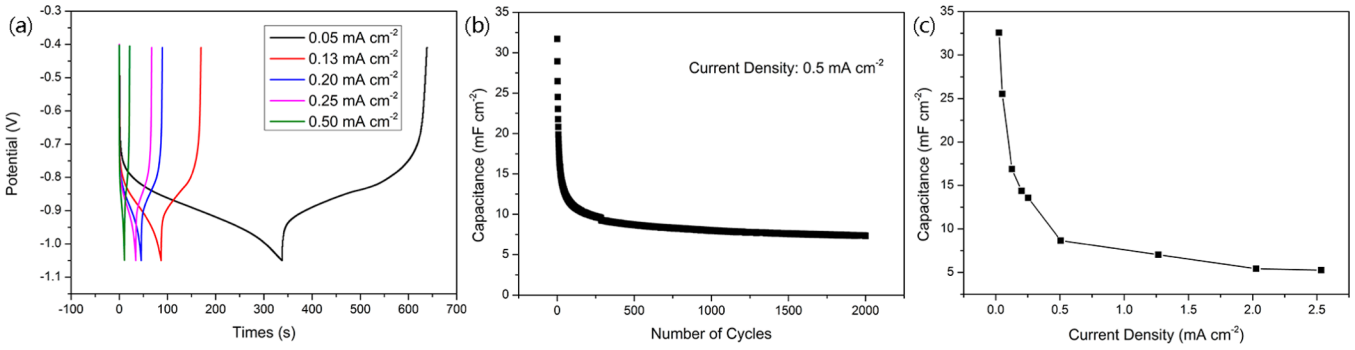

Figure 6. (a) Galvanostatic charge−discharge curves at different current densities. (b) Cycling performance of the $COF_{DAAQ\text{-}BTA}$-3DG composite at 0.5 mA/cm^2 in 1 mol/L KOH electrolyte. (c) Specific capacitance versus current density for $COF_{DAAQ\text{-}BTA}$-3DG composite.

appears at −0.888 V with a similar reduction current. The value of oxidation and reduction current peaks are much higher than the DAAQ monomer and the bare substrate 3DG, which indicates that the good alignment of $COF_{DAAQ\text{-}BTA}$ with the 3DG induced by the van der Waals epitaxy and covalent binding between DAAQ moieties allows more electrochemical active DAAQ moieties to be accessed. Figure 5a shows the CV curves of $COF_{DAAQ\text{-}BTA}$-3DG at different scan rates within the potential window of −0.4 V to approximately −1.05 V versus Ag/AgCl electrode obtain with a sample after charge−discharge cycling. A pair of pronounced redox peaks are located at ∼ −0.85 V and only one redox couple is observed. For reversible redox systems (electron transfer kinetics faster than mass transport), the same anodic and cathodic peak currents are expected for all scan rates.[26] As can be seen in Figure 5, cathodic peak and anodic peak currents of $COF_{DAAQ\text{-}BTA}$-3DG exhibit almost the same values at scan rates of 5−200 mV/s (Figure 5b), with the shape of CV curves for $COF_{DAAQ\text{-}BTA}$-3DG at different scan rates remains almost unchanged for the entire sweep, indicating a fast diffusion of electrolyte ions into the electrode.[4] However, the peak potential moved with the change of scan rate and the potential difference between the cathodic and anodic peak increases with the increase of scan rate. This indicates the process is a quasi-reversible rather than a reversible one.

Then the electrochemical properties of $COF_{DAAQ\text{-}BTA}$-3DG composite was also evaluated by charge−discharge experiments under different current densities (Figure 6a). These charge−discharge curves exhibit plateaus at −0.75 V to approximately −0.85 V, in accordance with the position of CV redox peaks. Their highly symmetric shapes reveal the high electrochemical reversibility and fast reaction kinetics.[27] The cycle performance of the composite was evaluated by galvanostatic charge−discharge test at 0.5 mA/cm^2 as shown in Figure 6b. It shows a rapid loss of the Faradaic specific capacitance, which reaches only 30% of the initial value (31.7 mF/cm^2) after 500 cycles. However, the value of specific capacitance is stabilized at around 7.6 mF/cm^2 in the rest of 2000 cycles. The capacitance of bare 3DG was also tested at 0.5 mA/cm^2 in 1 mol/L KOH electrolyte, which shows an average value of 0.6 mF/cm^2 (Figure S3). The double layer capacitance of 3DG accounts for only less than 3% to the total capacitance of the surface $COF_{DAAQ\text{-}BTA}$ −3DG composite (Figure S4). After 2000 cycles of galvanostatic charge−discharge at 0.5 mA/cm^2, the sample's capacitance was also estimated with different charge−discharge current densities. At each current density 10 charge−discharge cycles were measured, which reveals specific capacitance of ∼32.6 mF/cm^2 at 0.025 mA/cm^2 to ∼5.3 mF/cm^2 at 2.53 mA/cm^2 (Figure 6c). Moreover, as we vary the loading weight of the $COF_{DAAQ\text{-}BTA}$ on the 3DG to 0.098 and 0.427 mg/cm^2, the charge−discharge experiments reveal that the specific capacitance also increase nearly linearly (Figures S7 and S8). The peak currents of CV curves also indicate the same trend (Figure S9). This means that we can increase the capacitance per unit area through increasing the loading mass of COF.

We have estimated the accessible proportion of DAAQ moieties of $COF_{DAAQ\text{-}BTA}$-3DG composite relative to its theoretical maximum based on the loading weight. These calculations suggest that 13.5% of the DAAQ moieties are accessed at 0.025 mA/cm^2 (0.1 A/g if calculated against the

DOI: 10.1021/acsami.5b04185
ACS Appl. Mater. Interfaces 2015, 7, 17837−17843

weight of COF material) after cycling, which are much higher than the previous report where anthraquinone containing powder COF was binded with carbon black to serve as active material for capacitive storage, in their case only 2.5% of DAAQ moieties are accessed with a charge/discharge current density of 0.1 A/g.[12] We attribute this improvement to the good conductive contact between the $COF_{DAAQ\text{-}BTA}$ and 3DG, and the better contact of $COF_{DAAQ\text{-}BTA}$ with the electrolyte. The in situ preparation procedure in our work allows the van der Waals epitaxy growth of the $COF_{DAAQ\text{-}BTA}$ on 3DG surface, resulting in orientated growth of the $COF_{DAAQ\text{-}BTA}$ film, with the 2D COF in parallel with the graphene surface, allowing for overlap of π-orbitals of graphene and $COF_{DAAQ\text{-}BTA}$. Very recently, during the process of our research, Dichtel's group published another work where anthraquinone containing 2D COF thin films were grown on Au electrode via solvothermal condensation of DAAQ with 1,3,5-triformylphluroglucinal. In this case the 2D COF is oriented and about 20% of the DAAQ moieties are electrochemically accessible when charged in a 1 M H_2SO_4 media.[28]

As for the rapid loss of capacity during the cycling, we attributed it to the desorption of $COF_{DAAQ\text{-}BTA}$ in its reduced form due to repulsive electrostatic interaction accumulated during cycling,[8] and the dissolution of DAAQ monomers to electrolyte. The electrochemical reduction of the quinone groups of anthraquinone at pH 14 leads to the formation of a quinone dianion by a 2-electron process, which results in repulsive electrostatic interactions between the electrogenerated dianionic $COF_{DAAQ\text{-}BTA}$ layer and the negatively charged electrode surface.[8,29] Though the desorbing of the $COF_{DAAQ\text{-}BTA}$ layer is not as apparent as in the case of DAAQ monomer modified electrode, where orange color release may be observed during galvanostatic charge−discharge, our AFM characterization of the sample after cycling reveal partial desorption of the COF material, and this is also confirmed by the UV−vis spectra of the electrolyte solution (Figures S5 and S6). Thus, we attribute the loss of specific capacitance to the instability of the COF material during the charge−discharge process, and the accumulated electrostatic repulsion between different layers of $COF_{DAAQ\text{-}BTA}$ which results in desorption of the material and poor electric conductivity, and in turn reduce the accessible proportion of the DAAQ moieties.

CONCLUSION

In summary, we have prepared the $COF_{DAAQ\text{-}BTA}$-3DG composite via on-surface synthesis, which allows the oriented growth of $COF_{DAAQ\text{-}BTA}$ thin films on 3DG due to van der Waals epitaxy effect, facilitate the good conductive contact. Our results show that the good conductive contact of $COF_{DAAQ\text{-}BTA}$ to the 3DG significantly increased the accessible proportion of electrochemical active DAAQ moieties in comparison with powder 2D COFs. In aqueous alkaline electrolyte, the $COF_{DAAQ\text{-}BTA}$-3DG composite exhibits a large specific capacitance of 7.6 mF/cm^2. Long-term galvanostatic charge/discharge cycling experiments revealed a decrease of capacitance, which was attributed to the instability of the COF material and the accumulated electrostatic repulsion between different layers of $COF_{DAAQ\text{-}BTA}$ which results in poor electric conductivity. These results demonstrated that the $COF_{DAAQ\text{-}BTA}$-3DG composite could be a promising material to be used as negative electrode in an hybrid electrochemical capacitor or the polymer/air batteries based on alkaline electrolyte, though for practical applications the stability of the COF material still needs to be increased.

ASSOCIATED CONTENT

Supporting Information

The Supporting Information is available free of charge on the ACS Publications website at DOI: 10.1021/acsami.5b04185.

AFM images of three-dimensional graphene (3DG), electrochemical data of graphene, and $COF_{DAAQ\text{-}BTA}$-3DG composite with other loading mass (PDF)

AUTHOR INFORMATION

Corresponding Author

*E-mail: leisb@hit.edu.cn.

Author Contributions

The manuscript was written through contributions of all authors. All authors have given approval to the final version of the manuscript.

Notes

The authors declare no competing financial interest.

ACKNOWLEDGMENTS

This work is supported by the National Science Foundation of China (21173061, 21373070), and the Open Project of State Key Laboratory of Robotics and System (HIT) (SKLRS-2015-MS-11).

ABBREVIATIONS

COF, covalent organic framework
3DG, three-dimensional graphene
HOPG, highly oriented pyrolytic graphite
STM, scanning tunneling microscopy
AFM, atomic force microscope
DAAQ, 2,6-diaminoanthraquinone
BTA, benzene-1,3,5-tricarbaldehyde

REFERENCES

(1) Quan, M.; Sanchez, D.; Wasylkiw, M. F.; Smith, D. K. Voltammetry of quinones in unbuffered aqueous solution: Reassessing the roles of proton transfer and hydrogen bonding in the aqueous Electrochemistry of Quinones. *J. Am. Chem. Soc.* **2007**, *129* (42), 12847−12856.

(2) Zhou, Y. F.; Zhang, G. Q.; Chen, J.; Yuan, G. E.; Xu, L.; Liu, L. F.; Yang, F. L. A facile two-step electroreductive synthesis of anthraquinone/graphene nanocomposites as efficient electrocatalyst for O-2 reduction in neutral medium. *Electrochem. Commun.* **2012**, *22*, 69−72.

(3) Pognon, G.; Brousse, T.; Belanger, D. Effect of molecular grafting on the pore size distribution and the double layer capacitance of activated carbon for electrochemical double layer capacitors. *Carbon* **2011**, *49* (4), 1340−1348.

(4) Chen, X.; Wang, H. W.; Yi, H.; Wang, X. F.; Yan, X. R.; Guo, Z. H. Anthraquinone on Porous Carbon Nanotubes with Improved Supercapacitor Performance. *J. Phys. Chem. C* **2014**, *118* (16), 8262−8270.

(5) Choi, W.; Harada, D.; Oyaizu, K.; Nishide, H. Aqueous Electrochemistry of Poly(vinylanthraquinone) for Anode-Active Materials in High-Density and Rechargeable Polymer/Air Batteries. *J. Am. Chem. Soc.* **2011**, *133* (49), 19839−19843.

(6) Bekyarova, E.; Itkis, M. E.; Ramesh, P.; Berger, C.; Sprinkle, M.; de Heer, W. A.; Haddon, R. C. Chemical Modification of Epitaxial Graphene: Spontaneous Grafting of Aryl Groups. *J. Am. Chem. Soc.* **2009**, *131* (4), 1336.

DOI: 10.1021/acsami.5b04185
ACS Appl. Mater. Interfaces 2015, 7, 17837−17843

(7) Pognon, G.; Brousse, T.; Demarconnay, L.; Belanger, D. Performance and stability of electrochemical capacitor based on anthraquinone modified activated carbon. *J. Power Sources* **2011**, *196* (8), 4117−4122.
(8) Le Comte, A.; Brousse, T.; Belanger, D. Simpler and greener grafting method for improving the stability of anthraquinone-modified carbon electrode in alkaline media. *Electrochim. Acta* **2014**, *137*, 447−453.
(9) Furukawa, H.; Yaghi, O. M. Storage of Hydrogen, Methane, and Carbon Dioxide in Highly Porous Covalent Organic Frameworks for Clean Energy Applications. *J. Am. Chem. Soc.* **2009**, *131* (25), 8875−8883.
(10) Feng, X.; Ding, X. S.; Jiang, D. L. Covalent organic frameworks. *Chem. Soc. Rev.* **2012**, *41* (18), 6010−6022.
(11) Ding, S. Y.; Wang, W. Covalent organic frameworks (COFs): from design to applications. *Chem. Soc. Rev.* **2013**, *42* (2), 548−568.
(12) DeBlase, C. R.; Silberstein, K. E.; Truong, T. T.; Abruna, H. D.; Dichtel, W. R. beta-Ketoenamine-Linked Covalent Organic Frameworks Capable of Pseudocapacitive Energy Storage. *J. Am. Chem. Soc.* **2013**, *135* (45), 16821−16824.
(13) Xu, L. R.; Zhou, X.; Tian, W. Q.; Gao, T.; Zhang, Y. F.; Lei, S. B.; Liu, Z. F. Surface-Confined Single-Layer Covalent Organic Framework on Single-Layer Graphene Grown on Copper Foil. *Angew. Chem., Int. Ed.* **2014**, *53* (36), 9564−9568.
(14) Li, X. G.; Wang, Z. K.; Qiu, Y. F.; Pan, Q. M.; Hu, P. A. 3D graphene/ZnO nanorods composite networks as supercapacitor electrodes. *J. Alloys Compd.* **2015**, *620*, 31−37.
(15) Tanoue, R.; Higuchi, R.; Enoki, N.; Miyasato, Y.; Uemura, S.; Kimizuka, N.; Stieg, A. Z.; Gimzewski, J. K.; Kunitake, M. Thermodynamically Controlled Self-Assembly of Covalent Nanoarchitectures in Aqueous Solution. *ACS Nano* **2011**, *5* (5), 3923−3929.
(16) Guan, C. Z.; Wang, D.; Wan, L. J. Construction and repair of highly ordered 2D covalent networks by chemical equilibrium regulation. *Chem. Commun.* **2012**, *48* (24), 2943−2945.
(17) Xu, L. R.; Zhou, X.; Yu, Y. X.; Tian, W. Q.; Ma, J.; Lei, S. B. Surface-Confined Crystalline Two-Dimensional Covalent Organic Frameworks via on-Surface Schiff-Base Coupling. *ACS Nano* **2013**, *7* (9), 8066−8073.
(18) Zhang, J.; Wang, R.; Yang, X. C.; Lu, W.; Wu, X. D.; Wang, X. P.; Li, H.; Chen, L. W. Direct Observation of Inhomogeneous Solid Electrolyte Interphase on MnO Anode with Atomic Force Microscopy and Spectroscopy. *Nano Lett.* **2012**, *12* (4), 2153−2157.
(19) Basagni, A.; Colazzo, L.; Sedona, F.; Di Marino, M.; Carofiglio, T.; Lubian, E.; Forrer, D.; Vittadini, A.; Casarin, M.; Verdini, A.; Cossaro, A.; Floreano, L.; Sambi, M. Stereoselective Photopolymerization of Tetraphenylporphyrin Derivatives on Ag(110) at the Sub-Monolayer Level. *Chem. - Eur. J.* **2014**, *20* (44), 14296−14304.
(20) Elemans, J. A. A. W.; Lei, S. B.; De Feyter, S. Molecular and Supramolecular Networks on Surfaces: From Two-Dimensional Crystal Engineering to Reactivity. *Angew. Chem., Int. Ed.* **2009**, *48* (40), 7298−7332.
(21) Ivasenko, O.; Perepichka, D. F. Mastering fundamentals of supramolecular design with carboxylic acids. Common lessons from X-ray crystallography and scanning tunneling microscopy. *Chem. Soc. Rev.* **2011**, *40* (1), 191−206.
(22) Ciesielski, A.; El Garah, M.; Haar, S.; Kovaricek, P.; Lehn, J. M.; Samori, P. Dynamic covalent chemistry of bisimines at the solid/liquid interface monitored by scanning tunnelling microscopy. *Nat. Chem.* **2014**, *6* (11), 1017−1023.
(23) Liu, X. H.; Guan, C. Z.; Wang, D.; Wan, L. J. Graphene-Like Single-Layered Covalent Organic Frameworks: Synthesis Strategies and Application Prospects. *Adv. Mater.* **2014**, *26* (40), 6912−6920.
(24) Wang, J.; Ge, W.; Hou, Y.; Lu, Q. Scanning tunneling microscopy evidences for surface electron scattering by underlying atoms. *Carbon* **2015**, *84* (0), 74−81.
(25) Kibena, E.; Mooste, M.; Kozlova, J.; Marandi, M.; Sammelselg, V.; Tammeveski, K. Surface and electrochemical characterisation of CVD grown graphene sheets. *Electrochem. Commun.* **2013**, *35*, 26−29.
(26) Aguilo-Aguayo, N.; Bechtold, T. Characterisation of embroidered 3D electrodes by use of anthraquinone-1,5-disulfonic acid as probe system. *J. Power Sources* **2014**, *254*, 224−231.
(27) Zhao, F. P.; Wang, Y. Y.; Xu, X. N.; Liu, Y. L.; Song, R.; Lu, G.; Li, Y. G. Cobalt Hexacyanoferrate Nanoparticles as a High-Rate and Ultra-Stable Supercapacitor Electrode Material. *ACS Appl. Mater. Interfaces* **2014**, *6* (14), 11007−11012.
(28) DeBlase, C. R.; Hernandez-Burgos, K.; Silberstein, K. E.; Rodriguez-Calero, G. G.; Bisbey, R. P.; Abruna, H. D.; Dichtel, W. R. Rapid and Efficient Redox Processes within 2D Covalent Organic Framework Thin Films. *ACS Nano* **2015**, *9* (3), 3178−83.
(29) Jurmann, G.; Schiffrin, D. J.; Tammeveski, K. The pH-dependence of oxygen reduction on quinone-modified glassy carbon electrodes. *Electrochim. Acta* **2007**, *53* (2), 390−399.

DOI: 10.1021/acsami.5b04185
ACS Appl. Mater. Interfaces 2015, 7, 17837−17843